Light absorption and emissions inventory of humic-like substances from simulated rainforest biomass burning in Southeast Asia[☆]

Jiao Tang [a, e], Jun Li [a], Yangzhi Mo [a], Mahdi Safaei Khorram [a], Yingjun Chen [b], Jianhui Tang [c], Yanlin Zhang [d], Jianzhong Song [a], Gan Zhang [a, *]

[a] State Key Laboratory of Organic Geochemistry and Guangdong Key Laboratory of Environmental Protection and Resources Utilization, Guangzhou Institute of Geochemistry, Chinese Academy of Sciences, Guangzhou 510640, China
[b] Department of Environmental Science and Engineering, Fudan University, Shanghai 200092, PR China
[c] Key Laboratory of Coastal Environmental Processes and Ecological Remediation, Yantai Institute of Coastal Zone Research, Chinese Academy of Sciences, Yantai 264003, China
[d] Yale-NUIST Center on Atmospheric Environment, Nanjing University of Information Science and Technology, Nanjing 210044, China
[e] University of Chinese Academy of Sciences, Beijing 100049, China

ARTICLE INFO

ABSTRACT

Humic-like substances (HULIS) are complex mixtures that are highly associated with brown carbon (BrC) and are important components of biomass burning (BB) emissions. In this study, we investigated the light absorption, emission factors (EFs), and amounts of HULIS emitted from the simulated burning of 27 types of regionally important rainforest biomass in Southeast Asia. We observed that HULIS had a high mass absorption efficiency at 365 nm (MAE_{365}), with an average value of 2.6 ± 0.83 m^2 g^{-1} C. HULIS emitted from BB accounted for $65\% \pm 13\%$ of the amount of water-soluble organic carbon (WSOC) and $85\% \pm 10\%$ of the light absorption of WSOC at 365 nm. The EFs of HULIS from BB averaged 2.3 ± 2.1 g kg^{-1} fuel, and the burning of the four vegetation subtypes (herbaceous plants, shrubs, evergreen trees, and deciduous trees) exhibited different characteristics. The differences in EFs among the subtypes were likely due to differences in lignin content in the vegetation, the burning conditions, or other factors. The light absorption characteristics of HULIS were strongly associated with the EFs. The annual emissions (minimum−maximum) of HULIS from BB in this region in 2016 were 200−371 Gg. Furthermore, the emissions from January to April accounted for 99% of the total annual emissions of HULIS, which is likely the result of the burning activities during this season. The most significant emission regions were Cambodia, Burma, Thailand, and Laos. This study, which evaluated emissions of HULIS by simulating open BB, contributes to a better understanding of the light-absorbing properties and regional budgets of BrC in this region.

1. Introduction

Atmospheric aerosols play important roles in cloud formation, air quality, heterogeneous chemistry, Earth's radiation budget, and climate change (Dinar et al., 2006; Prasad et al., 2018; Xiang et al., 2017). Humic-like substances (HULIS), which make up a significant proportion (12%−45%) of the organics in aerosols (Baduel et al., 2010; Duarte et al., 2007; Lin et al., 2010a; Salma et al., 2010), are generally defined as the organic fraction in aerosols and

hydrometeors that exhibits chemical properties (UV−vis absorbance, fluorescence) similar to those of ubiquitous humic substances (Baduel et al., 2011; Graber and Rudich, 2006; Lin et al., 2010b). HULIS represent the hydrophobic fraction of water-soluble organic matter (WSOM) and account for 36%−63% of the carbon mass and more than 70% of the light absorption of WSOM in simulated biomass burning (BB) aerosols and ambient aerosols (Mo et al., 2018; Park and Yu, 2016). Hoffer et al. (2006) measured the spectral dependence of light absorption by HULIS (absorption Ångström exponent (AAE) ~6.5) in BB aerosol, which is generally characterized as brown carbon (BrC). Furthermore, Chen et al. (2016) determined that HULIS contributed ~ 40% of total BrC. HULIS can potentially affect the hygroscopicity of particles (Dinar et al., 2007). Thus, these substances not only affect atmospheric

---

heating and cooling through direct light absorption in the UV−visible spectrum but also affect indirect radiative forcing by activating cloud nucleation (Stone et al., 2009), and affect surface tension and photochemical processes (Wang et al., 2017; Zheng et al., 2013). HULIS, as a component of particulate matter (PM), may be active in generating reactive oxygen species (Chen et al., 2019; Lin and Yu, 2011). A very recent study also reported that HULIS can potentially induce human health risks (Ma et al., 2019).

HULIS in atmospheric aerosols mainly contain aromatic and aliphatic carboxylic acids, organosulfates (OS), carbohydrates, and other components (Claeys et al., 2012), and they are mainly derived from BB and fossil fuel burning, soil weathering, vehicle emissions, and secondary sources including oligomerization or polymerization and aerosol aging through gaseous precursors from biological and anthropogenic sources through an atmospheric chemical process (Voliotis et al., 2017; Win et al., 2018). Among the sources listed above, BB is generally considered one of the largest (Kumar et al., 2018; Voliotis et al., 2017; Zhou et al., 2018). Kuang et al. (2015) used positive matrix factorization analysis to determine 20%−28% of the HULIS-C (carbon mass of HULIS) derived from BB during winter in Guangzhou. Our prior carbon isotope analyses that more than 50% of HULIS-C is derived from non-fossil sources (e.g., BB and biogenic emissions) (Liu et al., 2018; Mo et al., 2018). Furthermore, it was reported that BB has important effects in Southeast Asia, where there were significant organic carbon (OC) emissions (530−1100 Gg) in 2016 and where the emission factors (EFs) of pollutants are higher than those in North America, South America, and Africa (Cui et al., 2018 and references therein). Recent studies have investigated the chemical properties, abundance, light absorption properties, sources, and structural properties of HULIS in smoke particles emitted from BB in a laboratory combustion chamber and field campaigns (Kumar et al., 2018; Mo et al., 2018; Park and Yu, 2016; Sengupta et al., 2018; Song et al., 2018; Zhou et al., 2018). However, limited studies have been conducted on the EFs of HULIS in source emissions, such as BB, which are important for estimating emission inventories and climate impacts.

Southeast Asia is one of three tropical rainforest systems worldwide and one of the most active areas for forest fires detected by the Moderate Resolution Imaging Spectroradiometer (MODIS). Streets et al. (2003) reported that BB in tropical forest fires accounted for 73% of the total burning activities every year in Southeast Asia. Recent studies showed that forest burning is the main source of air pollution in this region (Lee et al., 2017; Nakata et al., 2018). However, little is known about the influence of different vegetation types on the HULIS emitted from biomass fires in Southeast Asia. Thus, a comprehensive investigation of HULIS from BB emissions in this region is urgently needed.

An open burning simulation study is suitable for estimating the characteristics of emissions from the burning of different types of fuels (Roden et al., 2006). Analyses of HULIS data collected during simulated BB have suggested that determining the light absorption properties and amount of emissions of HULIS can improve our understanding of the profiles and regional budgets of BrC in this region. Therefore, we investigated BB emissions from regionally important fuels, including evergreen trees, deciduous trees, shrubs, and herbaceous vegetation, and characterized these properties in Southeast Asia. These results will help fill gaps in emission characteristic of HULIS in this highly BB-impacted region.

2. Materials and methods

2.1. Sampling

A newly designed sampling system consisting of a porous tube, a dilution tunnel, a residence time chamber, and PM samplers was used in this study. The detailed collection of smoke particles from simulated open BB has been reported elsewhere (Cui et al., 2018). Briefly, the biomass fuels were dried for several days until the moisture decreased to a very low value (about 10%, except for *Chaetocarpus castanocarpus* (23%)). The fuels (roughly $20 \times 3 \times 2$ cm^3) were ignited in a stainless-steel bowl, and the rising smoke was collected through the dilution system. For each biomass, about 1 kg of fuel was burned, and each combustion process lasted for 20 min. We performed three replicate burns for each fuel type. Smoke particles were collected from the time the fuel was ignited, and collection ended when the CO_2 levels dropped to atmospheric levels. Dilution ratios of each experimental process were calculated using the CO_2 concentrations before and after dilution. The sampling flow rate and average dilution ratio were 180 L min^{-1} and 2.1 ± 0.20, respectively. In total, 27 BB samples, including herbaceous vegetation (n = 3), evergreen tree (n = 14), deciduous tree (n = 5), and shrub (n = 5) burning samples, were collected in 8×10-inch quartz filters. The quartz filters for smoke collection were pre-baked at 450 °C for 5 h before sampling and then stored at −20 °C until analysis. Additional information about the sampling is provided in the Supplementary Data.

2.2. Chemical analysis

The separation of HULIS from WSOM was accomplished as follows. In brief, WSOM was obtained via ultrasonication of filter punches (area: 3.14 cm^2) with 40 mL of ultrapure water for 30 min at room temperature and then filtered with a 0.22-μm polytetrafluoroethylene (PTFE) membrane. A 20-mL WSOM solution was adjusted to pH 2 using hydrochloric acid (HCl). HULIS were isolated using a pretreated hydrophilic−lipophilic balanced (HLB) solid-phase extraction (SPE) cartridge (Oasis HLB, 30 mm, 200 mg/cartridge, Waters, USA) (Lin et al., 2010b; Varga et al., 2001). The inorganic ions and low molecular weight organic acids were removed by SPE (Lin et al., 2012). The HULIS retained on the SPE cartridge were eluted with 6 mL of methanol containing 2% ammonia and then dried under a gentle nitrogen flow. The HULIS were re-dissolved in 20 mL ultrapure water for further analysis. Quantification of HULIS was performed using a total organic carbon (TOC) analyzer (Vario TOC cube; Elementar, Germany).

2.3. UV−visible absorption spectra

The extract solution in a 1-cm path length quartz cell was subjected to analysis using a UV−visible spectrophotometer (UV-4802; Unico, China). The wavelengths used to characterize the UV−vis spectra were from 200 to 800 nm at a step size of 2 nm, and the contribution of the solvent to the UV−vis absorption spectra was subtracted. To characterize the chemical and absorption properties of HULIS, the AAE, Napierian absorption coefficients (α, m^{-1}), and mass absorption efficiency (MAE, m^2 g^{-1} C) were calculated, and these are presented in detail in the Supplementary Data.

2.4. EFs and emission amounts

Fuel-based EFs were obtained using a carbon-mass balance formula (Ferek et al., 1998). The underlying premise of this method is that all of the carbon combusted in a fire and released into the atmosphere is emitted into the smoke plume in five forms of carbon (CO_2, CO, CH_4, nonmethane hydrocarbons, and particulate carbon). In addition, during combustion, most of the carbon becomes CO and CO_2, and neglecting the other carbon species (CH_4, nonmethane hydrocarbons, and carbonaceous aerosols) may introduce an error of only 1−4% (Roden et al., 2006). Thus, we used

the optimization method to calculate the EFs (Cui et al., 2017; Cui et al., 2018):

$$EF_{HULIS} = \frac{\Delta X_{HULIS}}{\Delta CO_2} \cdot \frac{M_{HULIS}}{M_{CO_2}} \cdot EF_{CO_2} \tag{1}$$

$$EF_{CO_2} = \frac{C_F}{c(C_{CO}) + c(C_{CO_2}) + c(C_{OC}) + c(C_{EC})} \cdot c(CO_2) \cdot M_{CO_2} \tag{2}$$

where EF_{HULIS} and EF_{CO_2} (g kg^{-1} fuel) are the EFs for HULIS and CO_2, respectively; ΔX_{HULIS} and ΔCO_2 (mol m^{-3}) and M_{HULIS} and M_{CO_2} (g mol^{-1}) are the background-corrected concentrations and molecular weights of HULIS and CO_2, respectively; C_F (g C kg^{-1} fuel) is the amount of carbon before and after burning the biomass fuel; $c(C_{CO})$, $c(C_{CO_2})$, and $c(C_{OC})$, and $c(C_{EC})$ (g C m^{-3}) are the flue gas mass concentrations of CO, CO_2, OC, and elemental carbon (EC), respectively; and $c(CO_2)$ (mol m^{-3}) is the molar concentration of CO_2. Because the CO sensor did not function well in field sampling, we introduced the modified combustion efficiency (MCE), defined as an index of the relative amount of flaming and smoldering combustion occurring during a fire (Ward and Radke, 1993; Yokelson et al., 1997), which was calculated as the CO_2 concentration divided by the summed concentrations of CO_2 and CO (see Equation (3)). Our previous study summarized the MCE of BB, obtaining an average value of 0.91 ± 0.07, which was used for calculating the CO concentration (Cui et al., 2018 and references therein). This method was used in this study:

$$MCE = c(C_{CO_2}) / (c(C_{CO_2}) + c(C_{CO})) \tag{3}$$

where $c(C_{CO})$ and $c(C_{CO_2})$ are the flue gas mass concentrations of CO and CO_2 (g C m^{-3}), respectively.

In addition, HULIS emissions were calculated by estimating the emissions of HULIS from tropical rainforest burning in Southeast Asia on temporal and spatial scales in 2016. The emissions of HULIS from rainforest BB were defined by the following equation (Chang and Song, 2010):

$$E_{HULIS} = A \times B \times CF \times EF_{HULIS} \tag{4}$$

where E_{HULIS} is the emissions of HULIS (Gg). A is the burned area (m^2) in Southeast Asia in 2016, which was obtained from the MODIS active fire product (MCD45A1) with the Global Map data at a resolution of 500 m (https://e4ftl01.cr.usgs.gov/MOTA/); this was used to estimate the entire area that was burned in Southeast Asia in 2016. B is the aboveground available biomass density (kg m^{-2}), which consisted mainly of aboveground biomass fuels (forest, shrubland, and grassland) and was obtained from a previous study (Chang and Song, 2010 and reference therein). The CF (combustion factor), defined as the fraction of available fuels exposed to fire that are actually burned during combustion (Shi et al., 2014; Ward and Radke, 1993), was summarized in Cui et al. (2018). We used the values of 0.3 ± 0.09, 0.6 ± 0.18, and 0.9 ± 0.27 for coarse woodland (evergreen and deciduous trees), shrubs, and herbaceous vegetation, respectively, to calculate the emissions.

2.4.1. Uncertainty of emissions

Assessments of the amount of BB and the associated emissions remain highly uncertain. The large uncertainties associated with burned biomass estimates, particularly those associated with open burning, are caused by the uncertainties inherent in burned areas, fuel loads, combustion factors, and EFs (Ito and Penner, 2004). The uncertainty of HULIS emissions was measured by a propagation of error formula (Equations (5) and (6)), which is commonly used to

calculate the error:

$$U_h^2 = \sum U_{hi}^2 \tag{5}$$

$$(U_{hi}/AveE_{HULIS})^2 = (U_{Ai}/Ave_{Ai})^2 + (U_{EFi}/Ave_{EFi})^2 \\ + (U_{Bi}/Ave_{Bi})^2 + (U_{CFi}/Ave_{CFi})^2 \tag{6}$$

where U_h is the emission uncertainty of HULIS (Gg), and U_{hi} is the emission uncertainty of HULIS for vegetation i (i = coarse woodland (evergreen and deciduous trees), shrubs, and herbaceous vegetation). The $AveE_{HULIS}$ (Gg) is the product of the arithmetic mean of Avi_{Ai} (m^2), Ave_{EFi} (g kg^{-1} fuel), Ave_{Bi} (kg m^{-2}), and Ave_{CFi} based on Equation (4). In addition, U_{Ai}/Ave_{Ai} is the ratio of the standard deviation and average value of the burned area for vegetation i; U_{EFi}/Ave_{EFi} is the ratio of the standard deviation and average value of EFs for vegetation i; U_{Bi}/Ave_{Bi} is the ratio of the standard deviation and average value of aboveground biomass density for vegetation i; and U_{CFi}/Ave_{CFi} is the ratio of the standard deviation and average value of the combustion factor for vegetation i, respectively.

3. Results and discussion

3.1. Optical properties of HULIS in smoke particles of BB

AAE and MAE are important light absorption parameters that have been widely used to characterize the light properties of BrC. AAE is used to reflect the spectral dependence of BrC. Its values can be used to discriminate between black carbon (BC) and BrC. Generally, AAE values of BC are close to 1, and those of BrC are in excess of 1. Fig. S2 shows characteristic absorption spectra within the wavelength (λ) range of HULIS emitted from BB. The spectra exhibit a strong wavelength dependence. Previous studies of controlled combustion experiments reported high AAE values for alkaline-soluble HULIS$_{AS}$ (5.75 ± 0.11 for rice straw and 6.89 ± 0.13 for Chinese fir) and water-soluble HULIS$_{WS}$ ($6.20-8.13$) from primary BrC in BB smoke PM$_{2.5}$ (Fan et al., 2018) and for HULIS$_{WS}$ ($6.2-9.3$) from BB emissions (Park and Yu, 2016). In the present study, the fitted AAE (at $330-400$ nm) of HULIS emitted from BB was 6.7 ± 1.3 ($3.6-9.3$) (Table 1), and the correlation between $\ln(A_\lambda)$ and $\ln(\lambda)$ was greater than 0.99 ($p < 0.001$) (Fig. S2), which is characteristic of BrC. In fact, a significant proportion of the evidence for the atmospheric presence of BrC comes from the spectral properties of water extracts of aerosols (Chen et al., 2017; Zhang et al., 2013a). Shetty et al. (2019) indicated that these bulk solvent measurements of the AAE might not be representative of the spectral dependence of OC in the particle phase. However, the solvent-based method provides a direct measurement of BrC chromophore absorption without interference from light absorption by BC or other absorbers (Liu et al., 2013; Zhang et al., 2013a). AAE values are associated with sources, atmospheric processes (Li et al., 2016), fitting wavelength ranges, OC polarity (Chen and Bond, 2010), and extraction methods (Zhang et al., 2013a), and they vary widely at different locations. Saleh et al. (2013) found that photochemically aged organic aerosol (OA) emitted from BB exhibited higher AAE values than those of primary OA, and that the AAE increased upon processing. Martinsson et al. (2015) observed variable AAE values in different phases of combustion of wood burning.

We classified biomass fuels into four vegetation subtypes according to the properties of plants: herbaceous, evergreen trees, deciduous trees, and shrubs (Table 1). The AAE values of burning herbaceous plants (7.0 ± 0.44) and evergreen trees (6.9 ± 1.2) were slightly higher than those of deciduous trees (6.3 ± 1.9) and shrubs

Table 1
The EFs of HULIS, the ratios of HULIS-C/OC, HULIS-C/WSOC, and EC/OC, and light absorption of HULIS from BB emissions. The error indicates analytical uncertainty based on triplicate measurement.

Categories	Fuel name	EF_{HULIS} (g kg^{-1} fuel)	HULIS-C/OC (%)	HULIS-C/WSOC (%)	EC/OC (%)	AAE (330 $-$400 nm)	MAE_{250}(m^2 g^{-1} C)	MAE_{365}(m^2 g^{-1} C)	E_2/E_3
Herbaceous	Musa nana Lour.	3.7 ± 0.12	30% ± 1.0%	74% ± 3.3%	6.5%	7.1 ± 0.012	8.3 ± 0.004	1.8 ± 0.009	4.6 ± 0.025
	Rhynchelytrum repens	2.2 ± 0.070	41% ± 1.3%	87% ± 2.2	11%	7.3 ± 0.12	8.7 ± 0.0014	1.7 ± 0.023	5.0 ± 0.061
	Eupatorium odoratum L.	0.60 ± 0.023	34% ± 1.4%	64% ± 3.3%	33%	6.5 ± 0.12	11 ± 0.068	2.5 ± 0.065	4.5 ± 0.088
Shrubs	Lasiococca comberi Haines	0.93 ± 0.032	7.0% ± 0.24%	68% ± 3.5%	0.58%	6.8 ± 0.11	7.8 ± 0.035	2.2 ± 0.006	3.6 ± 0.026
	Pseudostachyum Polymorphum	1.2 ± 0.032	38% ± 1.0%	71% ± 2.7%	38%	6.3 ± 0.088	8.7 ± 0.030	2.3 ± 0.017	3.7 ± 0.037
	Rauvolfieae verticillata*	0.32 ± 0.038	26% ± 3.0%	39% ± 5.7%	57%	4.1 ± 0.29	18 ± 3.3	5.1 ± 0.45	3.5 ± 0.36
	Rauvolfieae verticillata	3.5 ± 0.032	55% ± 0.50%	84% ± 1.3%	13%	6.9 ± 0.068	8.1 ± 0.62	2.1 ± 0.317	3.9 ± 0.32
	Trema tomentosa (Roxb.) H. Hara	1.1 ± 0.016	38% ± 0.56%	68% ± 1.0%	9.0%	8.1 ± 0.047	11 ± 0.008	3.1 ± 0.006	3.5 ± 0.006
Evergreen trees	Castanopsis Spach	4.6 ± 0.090	32% ± 0.63%	76% ± 1.8%	7.5%	8.0 ± 0.14	9.4 ± 0.011	1.6 ± 0.037	5.7 ± 0.12
	Antiaris toxicaria Lesch	5.3 ± 0.19	40% ± 1.4%	87% ± 5.0%	7.0%	8.9 ± 0.023	7.4 ± 0.002	1.3 ± 0.003	5.8 ± 0.014
	Toona ciliata Roem.	3.5 ± 0.11	24% ± 0.80%	50% ± 1.1%	7.9%	6.3 ± 0.35	11 ± 2.3	2.7 ± 0.63	4.0 ± 0.010
	Duabanga grandiflora	1.1 ± 0.041	31% ± 1.1%	47% ± 1.6%	18%	5.6 ± 0.19	13 ± 3.5	3.8 ± 1.1	3.4 ± 0.023
	Anthocephalus chinensis	1.1 ± 0.040	39% ± 1.4%	72% ± 2.4%	13%	7.5 ± 0.055	8.7 ± 0.008	2.0 ± 0.005	4.3 ± 0.009
	Macaranga denticulata	2.1 ± 0.044	28% ± 0.58%	57% ± 0.50%	18%	6.7 ± 0.020	13 ± 0.008	3.6 ± 0.017	3.7 ± 0.015
	Litchi chinensis Sonn.	0.47 ± 0.014	27% ± 0.77%	53% ± 2.1%	12%	6.4 ± 0.011	13 ± 0.007	2.8 ± 0.020	4.6 ± 0.031
	Pinus kesiya var. langbianensis	0.78 ± 0.010	31% ± 0.42%	58% ± 1.5%	30%	6.7 ± 0.083	12 ± 0.018	3.1 ± 0.023	3.8 ± 0.034
	Paramichelia baillonii	1.5 ± 0.044	29% ± 0.87%	64% ± 2.3%	16%	6.6 ± 0.077	13 ± 3.3	3.5 ± 0.93	3.7 ± 0.056
	PterospermummenglunenseHsue	2.8 ± 0.062	33% ± 0.75%	54% ± 4.0%	7.0%	6.6 ± 0.022	11 ± 0.007	3.1 ± 0.002	3.7 ± 0.003
	Cassia siamea Lam.	1.6 ± 0.033	35% ± 0.73%	53% ± 0.40%	24%	6.2 ± 0.028	11 ± 0.007	2.9 ± 0.006	3.8 ± 0.006
	Baccaurea ramiflora Lour	1.7 ± 0.061	37% ± 1.3%	55% ± 1.9%	23%	5.4 ± 0.058	10 ± 0.023	3.1 ± 0.017	3.4 ± 0.017
	Chaetocarpus castanocarpus	8.6 ± 0.065	34% ± 0.25	54% ± 3.6%	3.3%	9.3 ± 1.5	9.4 ± 0.99	2.2 ± 0.50	4.4 ± 0.63
	Citrus maxima	0.62 ± 0.007	31% ± 0.33%	48% ± 2.9%	16%	6.0 ± 0.017	13 ± 0.008	3.0 ± 0.027	4.4 ± 0.039
Deciduous trees	Melia azedarach	1.8 ± 0.056	25% ± 0.79%	53% ± 2.0%	7.9%	6.3 ± 0.014	12 ± 0.009	2.8 ± 0.011	4.1 ± 0.018
	Bischofia polycarpa	6.9 ± 0.072	43% ± 0.44%	78% ± 3.6%	5.4%	7.0 ± 0.076	8.3 ± 0.013	2.0 ± 0.020	4.1 ± 0.003
	Broussonetia papyrifera*	0.89 ± 0.019	7.9% ± 0.17%	78% ± 2.0%	5.0%	5.9 ± 0.094	10 ± 0.036	2.6 ± 0.017	3.9 ± 0.027
	Broussonetia papyrifera	1.7 ± 0.024	21% ± 0.30%	73% ± 1.8%	7.8%	8.9 ± 0.042	6.8 ± 0.012	1.4 ± 0.008	5.0 ± 0.022
	Hevea brasiliensis	0.63 ± 0.006	54% ± 0.49%	82% ± 5.4%	49%	3.6 ± 0.46	8.4 ± 1.4	3.1 ± 0.552	2.7 ± 0.034

Where the levels of OC and WSOC were described in our other study (Tang et al., 2020); Note that the "*" is representative of the twig of this tree.

(6.4 ± 1.5) (Fig. 1a). It seemed that the fuel types were responsible for the different AAE values. Here, we introduce the EC/OC ratio, which is used as an indicator of fire conditions. Recent studies comparing MCE and EC/OC have indicated that EC/OC is key to understanding aerosol absorption properties (Lu et al., 2015; Pokhrel et al., 2016). The correlation clearly showed that the AAE of HULIS from BB is dependent on the burn conditions (Fig. S3a). A similar result was observed in the study of Xie et al. (2017). In addition, Chen and Bond (2010) inferred that higher AAE values are associated with weakly absorbing particles. Additionally, previous study has indicated that pH has a significant influence on light absorption properties (Mo et al., 2017). Thus, to eliminate the effect of pH, we adjusted the pH of the HULIS solution to that of WSOM using dilute HCl or NaOH. We found that the AAE values of HULIS were lower than those of WSOM, indicating that HULIS have a higher degree of conjugation. Similar results have been observed in many other studies (Li et al., 2018; Liu et al., 2018; Mo et al., 2018) (Table S1). Generally, BrC exhibits significant absorption at 365 nm, a wavelength long enough to avoid the influences from non-organic compounds (e.g., nitrate) (Hecobian et al., 2010; Xie et al., 2019). In this study, HULIS accounted for 85 ± 10% of the absorption at 365 nm by WSOM (Fig. 2), which was comparable with a previously reported rate of 80 ± 6.1% of the WSOC absorption (Mo et al., 2018). Park and Yu (2016) found that light absorption by WSOM from BB had a stronger relationship with HULIS than with non-HULIS. Thus, HULIS are important absorption components of WSOM. Moreover, a clear shoulder in the region of 250−300 nm was observed in HULIS of smoke particles emitted from BB. This is generally attributed to π−π* electron transitions in moieties containing C=C and C=O double bonds (Domeizel et al., 2004).

MAE can reflect light absorption ability and is defined as the ratio of the light absorption by each extract to the mass concentration. The MAE value of HULIS at 365 nm (MAE_{365}) was 2.6 ± 0.83 m^2 g^{-1} C for BB emissions (Table 1 and Fig. 1c). For the four vegetation subtypes, HULIS from burning shrubs had the highest light absorption capacity (3.0 ± 1.3 m^2 g^{-1} C), followed by those from evergreen trees (2.8 ± 0.74 m^2 g^{-1} C), deciduous trees (2.4 ± 0.69 m^2 g^{-1} C), and herbaceous plants (2.0 ± 0.45 m^2 g^{-1} C). A study by Saleh et al. (2014) reported that the absorptivity of aerosols emitted from BB depended largely on the burn conditions, not the fuel type. In addition, Chen and Bond (2010) indicated that MAE values were mainly affected by pyrolysis temperature and that the difference caused by temperature was larger than the differences resulting from wood type and wood size. A significant correlation between EC/OC and MAE_{365} of HULIS further confirmed that the light absorption of HULIS from BB emissions depended on the burn conditions, as measured by EC/OC (Fig. S3a). In this study, the MAE_{365} values emitted from BB were much higher than those from water extracts (0.16−2.09 m^2 g^{-1} C) (Sengupta et al., 2018) and water-soluble HULIS (1.12−1.60 m^2 g^{-1} C) (Fan et al., 2018) from BB emissions, as well as those of ambient aerosols including WSOC and HULIS (1.0 ± 0.3 and 0.8 ± 0.3 m^2 g^{-1} C, respectively) of PM$_{2.5}$ in Korea (Park et al., 2018), WSOC (1.22 ± 0.11 m^2 g^{-1} C) of PM$_{2.5}$ in Beijing (Cheng et al., 2016), and water-soluble HULIS from coal combustion (0.5−1.0 m^2 g^{-1} C) (Li et al., 2018), suggesting that water-soluble HULIS derived from BB have strong light-absorbing capacity. Previous work indicated that the MAE value of WSOC was almost three times higher in BB periods than in non-BB periods (Hecobian et al., 2010). This phenomenon indicates that primary WSOC or HULIS from BB can significantly affect the light-absorbing abilities of organic aerosols in the atmospheric environment. Furthermore, the higher absorption efficiency of biomass smoke may be associated with the presence of polar aromatic compounds, such as phenolic species from lignin pyrolysis (Duarte et al., 2007; Phillips and Smith, 2014).

The ratio of MAE_{250} to MAE_{365} (E_2/E_3), which is negatively correlated with aromaticity and molecular size, has been successfully applied to characterize the chemical properties of HULIS (Chen
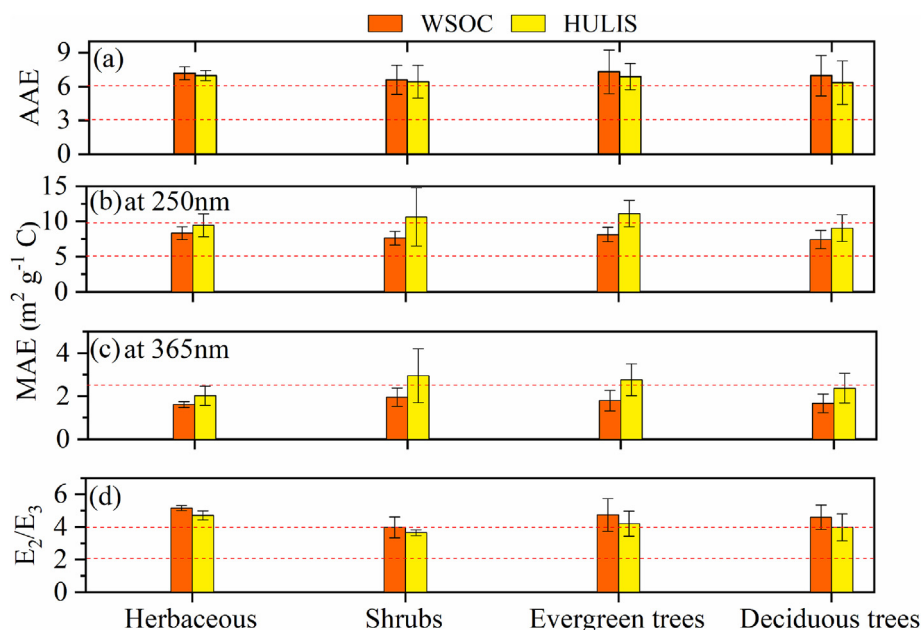
Fig. 1. The AAE values (a), MAE at 250 and 365 nm (b and c, respectively), and E_2/E_3 values (d) for the WSOC, HULIS emitted from BB, respectively. Where the MAE_{365} of WSOC was described in our other study (Tang et al., 2020).
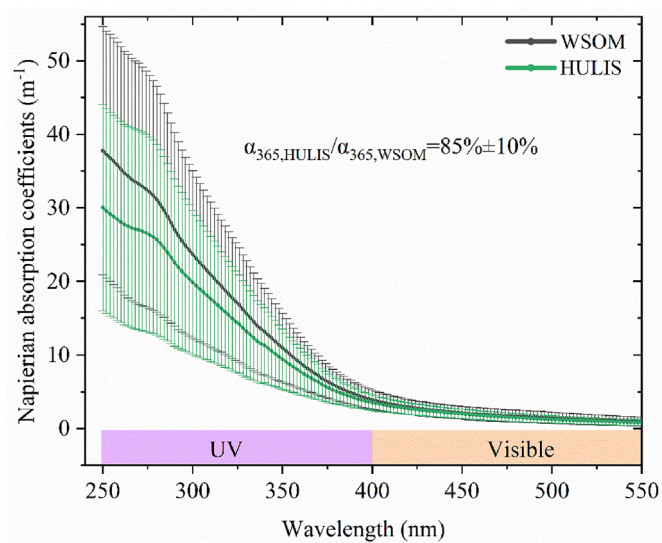

Fig. 2. Mean of light absorption of WSOM and HULIS and mean of the relative contributions of HULIS to WSOM absorption from BB emissions.

et al., 2016; Fan et al., 2012). Table 1 and Fig. 1d show that the E_2/E_3 values of HULIS were 4.1 ± 0.71 for overall BB samples, 4.7 ± 0.27 for herbaceous plants, 3.6 ± 0.18 for shrubs, 4.2 ± 0.77 for evergreen trees, and 4.0 ± 0.82 for deciduous trees, implying that these BB-derived HULIS had similar aromaticity and molecular size ($p > 0.05$, t-test). These results are consistent with our previous study that analyzed smoke particles from one herbaceous plant and one deciduous tree and obtained a similar compositional structure using Fourier-transform ion cyclotron resonance mass spectrometry (Tang et al., 2020). In contrast with WSOC (Fig. 1), HULIS had higher MAE_{365} and lower E_2/E_3 values, indicating the larger molecular size and higher aromaticity of HULIS. This result is consistent with the result that the strongly light-absorbing component of the water-soluble BrC was concentrated in the isolated HULIS (Mo

et al., 2017), and the HLB method used in this study was favorable for isolating high UV-absorbing, more aromatic compounds (Fan et al., 2012). The E_2/E_3 values in this study were comparable to those of primary HULIS emitted from the combustion of biomass (5.8 ± 0.5, 4.5 ± 0.2, and 4.4 ± 0.3 for combustion of rice straw, corn straw, and pine branches, respectively), lower than that of primary HULIS emitted from the combustion of coal (14.7 ± 0.7) (Fan et al., 2016), and lower than that of atmospheric HULIS (5.8 ± 0.4 and 11.2 ± 1.4 for HULIS-n and HULIS-a, i.e., of neutral and acidic nature at the elution step, respectively) (Chen et al., 2016).

3.2. HULIS EFs

The EF_{HULIS} emitted from the burning of 27 types of tropical plants are presented in Table 1. The average EF_{HULIS} was 2.3 ± 2.1 g kg^{-1} fuel, and the range was $0.32-8.6$ g kg^{-1} fuel. A wide range of EFs was observed for the burning of different fuels, which was probably due not only to the burn conditions but also to other factors. Fig. S3b shows the relationship between the EFs of HULIS and EC/OC ($R^2 = 0.23$), showing that EF_{HULIS} was dependent on the burn conditions. However, the weak correlation suggested that something other than fire conditions might influence the EFs of HULIS emitted from BB. Mcmeeking et al. (2009) indicated that fuels with higher moisture burned with lower MCE, and that factors other than fuel moisture, such as the fuel mass and burning of different plant components, affect the MCE. Their results showed that EFs were negatively correlated with MCE and increased with increasing contributions from smoldering-phase combustion. Similar results were observed in a previous study (Ferek et al., 1998). This indicates that the EFs may be affected by various factors. The emission profiles of HULIS from the burning of the four vegetation subtypes were different. The average EF_{HULIS} values were 2.1 ± 1.5 g kg^{-1} fuel for herbaceous plants, 1.4 ± 1.2 g kg^{-1} fuel for shrubs, 2.6 ± 2.3 g kg^{-1} fuel for evergreen trees, and 2.4 ± 2.6 g kg^{-1} fuel for deciduous trees (Fig. 3). The lignin content of the vegetation is likely another reason for the different EFs. Lignin reportedly accounts for $7.4-12.2\%$ of the lignocellulose in herbaceous plants and $21-25\%$ in deciduous and evergreen trees
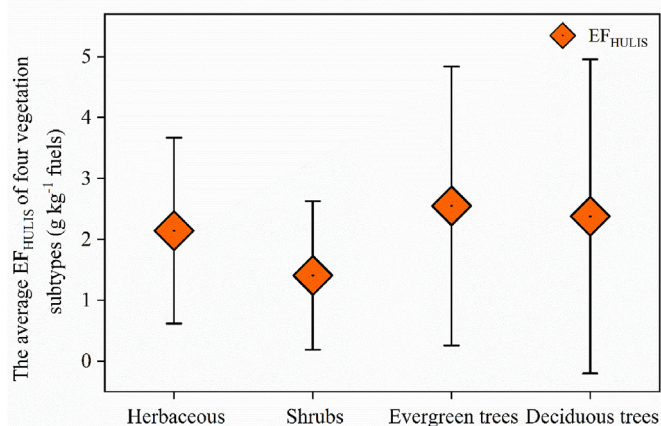
Fig. 3. The average EF$_{HULIS}$ of four Vegetation sub-types burning in Southeast Asia.

(Cui et al., 2018; Guo et al., 2008). This may be the reason that the EFs of HULIS emitted from the burning of deciduous and evergreen trees were higher than those of HULIS emitted from herbaceous plants. HULIS EFs for vegetation burning varied widely, as indicated by the high standard deviations associated with the data. The different EF$_{HULIS}$ of the four types of tropical forest vegetation in this study illustrated that there was large uncertainty when calculating the emissions of HULIS using only a single EF. In addition, we found that the lowest EFs of HULIS, emitted from shrubs, corresponded to the highest MAE$_{365}$ and the lowest E$_2$/E$_3$ values (described previously), implying lower EFs but higher light absorption ability of the HULIS.

The ratios of HULIS-C to OC and to WSOC for each biomass type are summarized in Table 1. The average HULIS-C/WSOC ratio in the present study was 65% ± 13%, which is generally within the range of 24%–72% of the ambient HULIS-C/WSOC ratio (Tan et al., 2016). The atmospheric HULIS-C/WSOC is influenced by differences in the major formation processes and increases from secondary formation (Park and Yu, 2016). The ratios of HULIS-C to WSOC exhibited distinct differences among the four vegetation fuels, being almost 10%–20% higher in herbaceous (75% ± 11%) and deciduous trees (72% ± 12%) than in shrubs (66% ± 17%) and evergreen trees (59% ± 12%). However, relatively consistent HULIS-C/OC ratios (from 30% ± 18% in deciduous trees to 35% ± 5.6% in herbaceous plants) were observed among the four vegetation fuels. The average value of the HULIS-C/WSOC ratio in the present study was comparable with the ratio of rice straw (63%) and higher than that of pine needles (36%) and sesame stems (51%) from simulated BB aerosols (Park and Yu, 2016). The highly BB-impacted region exhibited a HULIS-C/WSOC ratio of up to 63%–70% (Salma et al., 2010). HULIS have been reported as the dominant components of WSOC worldwide and comprise almost 72% of the latter (Kiss et al., 2002). In addition, a significant fraction of HULIS-C/WSOC was found in other chamber experiments and ambient aerosols, such as coal combustion (30%–63%) (Li et al., 2018), aerosol (32%–43%) (Voliotis et al., 2017), and Arctic aerosol (3.0%–16%) (Nguyen et al., 2014). However, direct comparisons of HULIS among different studies are hampered by the different methods used for isolating and quantifying HULIS (Nguyen et al., 2014). The HULIS-C/OC ratio (32% ± 11%) in the present study was higher than the ratios (27% ± 3.0% during the day and 20% ± 3.0% at night) in PM$_{10}$ in the Indo-Gangetic Plain (Kumar et al., 2018) but lower than that (36% ± 7.0%) in PM$_{2.5}$ from Weizhou Island (Zhou et al., 2018). Lin et al. (2010a) observed that HULIS-C/OC ratios were much higher

in BB-affected ambient samples (61% ± 16% and 62% ± 10% for suburban and urban samples, respectively) than in fresh BB samples, probably due to multiple pathways leading to secondary formation of HULIS as BB smoke ages in the atmosphere.

The relationships between the EFs of HULIS and those of PM, OC, EC, WSOC, and non-HULIS (non-HULIS = WSOC − HULIS) emitted from BB are presented in Fig. 4a and b and Table S2. For all BB samples, the EF$_{HULIS}$ values were significantly associated with the EFs of PM, OC, and WSOC, with R^2 values of 0.84, 0.76, and 0.92, respectively, but weakly correlated with the EF of EC (R^2 = 0.17). This can be explained by the MCE value. A decrease in MCE (more smoldering) resulted in an increase in OC and a decrease in EC emissions, but there was a slight increase in EC particle production compared with OC in the flaming combustion process (Jen et al., 2019). Due to the strong light absorption and high emission of HULIS, the relationship between EF$_{HULIS}$ and the optical properties was assessed (Fig. 4c and Table S2). EF$_{HULIS}$ was positively associated with α_{280} (P < 0.01) and α_{365} (P < 0.01), indicating the important relationship between EFs and the light absorption of HULIS.

3.3. HULIS emissions in Southeast Asia

Through calculations using the equation considering EF$_{HULIS}$ along with BB area, fuel load, and CF, we determined the annual HULIS emissions from BB in Southeast Asia. Table 2 shows that the emissions of HULIS from BB in 2016, totaling 223 Gg, contributed one-third of the OC emissions (687 Gg) in this region (Cui et al., 2018), indicating that HULIS are an important component of BB emissions in Southeast Asia. However, uncertainty in BB emissions is mainly associated with biomass amount, burning fraction, and EFs (Zhang et al., 2013b). Thus, we assumed that the total uncertainties from the MODIS burned-area product and the combustion factor were 20% and 30%, respectively, as reported by previous studies (Hyer and Reid, 2009; Jain et al., 2006). The standard deviations of the mean values of EF$_{HULIS}$ estimated in this study were 92%, 87%, and 71% for forest, shrub, and herbaceous burning, respectively. Finally, we estimated the emissions of HULIS (minimum to maximum), which ranged from 200 to 371 Gg year^{-1}. Due to the lack of EFs and emissions of HULIS in other studies, we roughly calculated the HULIS emissions by multiplying by a conversion rate of one-third of the OC emissions. We observed that HULIS emissions in Southeast Asia in 2016 were higher than the calculated HULIS emissions (137 Gg for average annual L3JRC-based emissions and 130 Gg for average annual MCD45A1-based emissions) from BB in Southeast Asia from 2000 to 2006 (Chang and Song, 2010), and the calculated HULIS emissions (81 Gg in 2000 and a projection of 54 Gg in 2020) estimated for household coal combustion in China (Chen et al., 2009).

In this region (Fig. 5a), Cambodia emitted the highest amount of HULIS, with an annual total of 93 Gg, followed by Burma (79 Gg) and Thailand (32 Gg), contributing 42%, 35%, and 14% of the total HULIS emissions in 2016, respectively. In addition, assessment of seasonal changes showed that the HULIS emissions in January (71 Gg), February (70 Gg), and March (65 Gg), accounting for 32%, 32%, and 29% of the total annual emissions, respectively, were higher than those in other months. There is no doubt that high emissions of HULIS were observed in mainland Southeast Asia during January to March, which is consistent with the results of Lee et al. (2017), in which higher PM$_{2.5}$ concentrations were found in this region during February to April from 2003 to 2014. Aside from the months of January−March, the emission of HULIS in April was relatively high at 15 Gg, accounting for 6.6% of the total annual
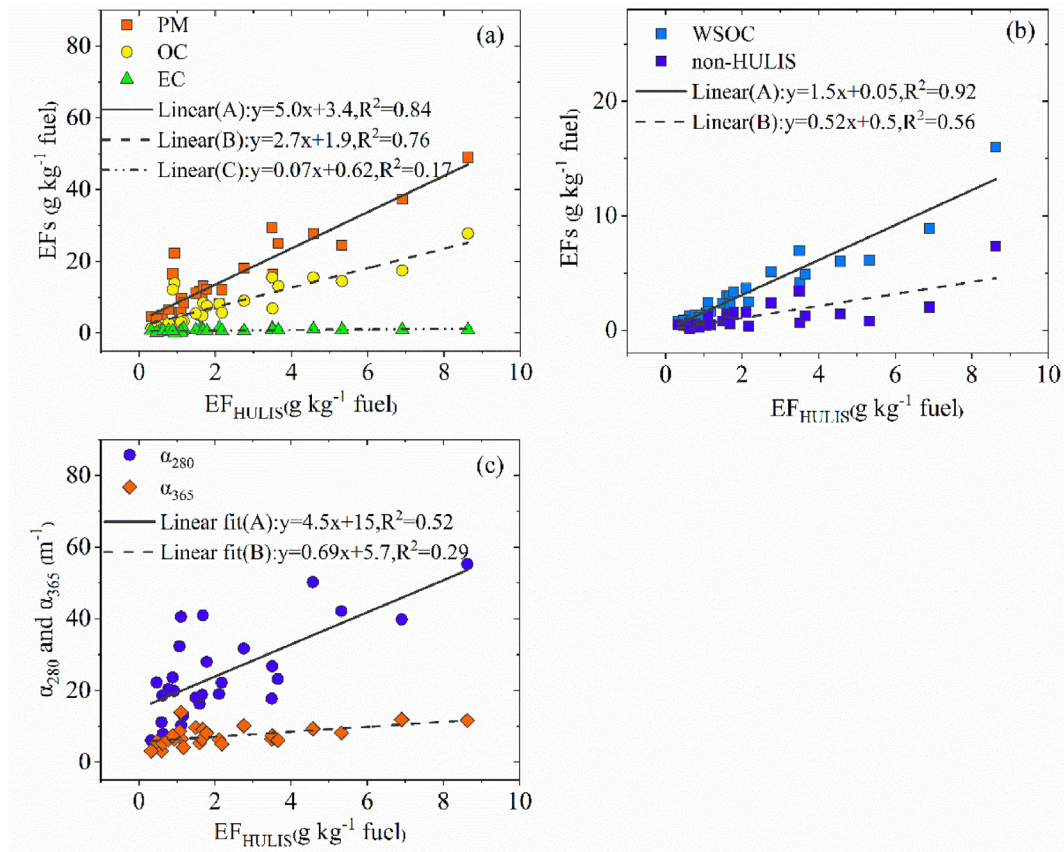
Fig. 4. Relationships between EF_{HULIS} and (a, b) EF_{PM}, EF_{OC}, EF_{EC}, EF_{WSOC}, and $EF_{non-HULIS}$, and (c) light absorption of HULIS from BB emissions.

Table 2
Emissions of HULIS from rainforest BB in Southeast Asia in 2016.

Month in 2016	Burning area (km^2)	E_{HULIS} (Gg)
January	4044	70.9
February	4605	70.4
March	4901	65.2
April	1031	14.6
May	33.0	0.58
June	1.16	0.031
July	2.38	0.064
August	8.89	0.24
September	8.23	0.22
October	0.20	0.0055
November	1.68	0.027
December	19.5	0.30
Sum	14,657	223
Uncertainty	2931	200—371 (minimum—maximum)

emissions. We further determined that the HULIS emissions from January—April accounted for 99% of the total annual HULIS emissions, which was explained by a previous study that concluded that such temporal variations were attributable to climate and agricultural activities (Cui et al., 2018). Streets et al. (2003) showed that Southeast Asia exhibits a high degree of BB in the spring. This finding was also supported by densely distributed active fire spots obtained from MODIS (Fig. S4). For the fire season of BB, which lasts from February to April, we calculated the relative contributions of nine countries to the total monthly emissions and plotted the results in Fig. 5b. The results revealed that Cambodia emitted considerable HULIS in January and February, accounting for 82%

and 47% of the total monthly emissions, respectively. This may be due to the extensive burning that occurred, which was the main source for high HULIS emissions in Cambodia in January (84% of the total burned area) and February (42% of the total burned area). The significant HULIS emissions in February—April, but not January, in Burma and Thailand may have been due to clearing land with fire before spring cultivation.

4. Conclusions

This is the first study to use simulated rainforest BB to calculate the emissions and light absorption of HULIS emitted in Southeast Asia. We observed that the derived water-soluble HULIS exhibited strong light absorption, and as a hydrophobic component of WSOM, accounted for 65% $\pm$ 13% of the WSOC from BB emissions, contributing 85 $\pm$ 10% of the light absorption of WSOM at 365 nm. We also observed that the EFs of HULIS differed among the four vegetation subtypes, likely due to differences in lignin content, burning conditions, or other factors. The total emission of HULIS from BB in Southeast Asia in 2016 was 223 Gg. Cambodia made the highest contribution to this amount, with an annual total of 93 Gg, followed by Burma (79 Gg) and Thailand (32 Gg). The seasonal distribution showed that the emissions from January to April accounted for 99% of the total annual HULIS emissions. The high amount of emissions and strong light absorption of HULIS from BB in Southeast Asia indicated that BB-derived HULIS have an important influence on the regional radiation budget and climate change. These results will provide new insights into the profiles of HULIS in this region.
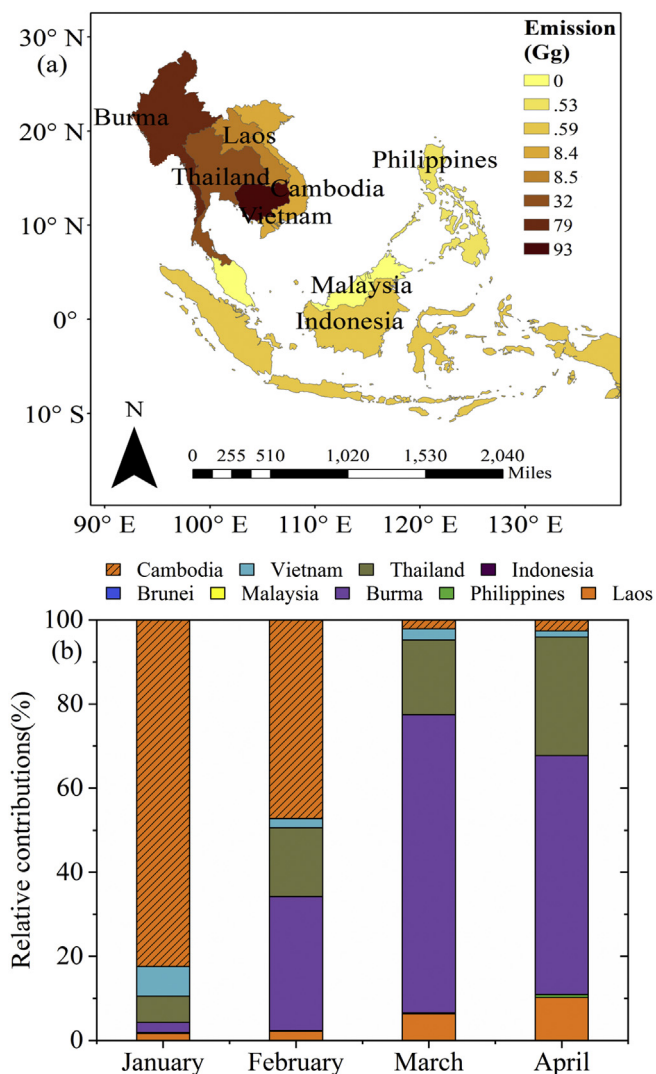
Fig. 5. Emissions of HULIS in Southeast Asia (a) and the relative contributions of HULIS to total emissions amount from January to April (b) from BB emissions in nine countries in 2016.

Declaration of competing interest

The authors declare that they have no known competing financial interests or personal relationships that could have appeared to influence the work reported in this paper.

CRediT authorship contribution statement

Jiao Tang: Conceptualization, Methodology, Software, Data curation, Writing - original draft. **Jun Li:** Supervision, Writing - review & editing. **Yangzhi Mo:** Conceptualization, Methodology, Software. **Mahdi Safaei Khorram:** Validation. **Yingjun Chen:** Visualization, Investigation. **Jianhui Tang:** Software. **Yanlin Zhang:** Validation. **Jianzhong Song:** Validation. **Gan Zhang:** Supervision.

Acknowledgements

Appendix A. Supplementary data

Supplementary data to this article can be found online at https://doi.org/10.1016/j.envpol.2020.114266.

References

Baduel, C., Monge, M.E., Voisin, D., Jaffrezo, J.L., George, C., Haddad, I.E., Marchand, N., D'Anna, B., 2011. Oxidation of atmospheric humic like substances by ozone: a kinetic and structural analysis approach. Environ. Sci. Technol. 45, 5238–5244.

Baduel, C., Voisin, D., Jaffrezo, J.L., 2010. Seasonal variations of concentrations and optical properties of water soluble HULIS collected in urban environments. Atmos. Chem. Phys. 10, 4085–4095.

Chang, D., Song, Y., 2010. Estimates of biomass burning emissions in tropical Asia based on satellite-derived data. Atmos. Chem. Phys. 10, 2335–2351.

Chen, Q., Ikemori, F., Mochida, M., 2016. Light absorption and excitation-emission fluorescence of urban organic aerosol components and their relationship to chemical structure. Environ. Sci. Technol. 50, 10859–10868.

Chen, Q., Ikemori, F., Nakamura, Y., Vodicka, P., Kawamura, K., Mochida, M., 2017. Structural and light-absorption characteristics of complex water-insoluble organic mixtures in urban submicrometer aerosols. Environ. Sci. Technol. 51, 8293–8303.

Chen, Q., Wang, M., Wang, Y., Zhang, L., Li, Y., Han, Y., 2019. Oxidative potential of water-soluble matter associated with chromophoric substances in $PM_{2.5}$ over Xi'an, China. Environ. Sci. Technol. 53, 8574–8584.

Chen, Y., Bond, T.C., 2010. Light absorption by organic carbon from wood combustion. Atmos. Chem. Phys. 10, 1773–1787.

Chen, Y., Zhi, G., Feng, Y., Liu, D., Zhang, G., Li, J., Sheng, G., Fu, J., 2009. Measurements of black and organic carbon emission factors for household coal combustion in China: implication for emission reduction. Environ. Sci. Technol. 43, 9495–9500.

Cheng, Y., He, K.-b., Du, Z.-y., Engling, G., Liu, J.-m., Ma, Y.-l., Zheng, M., Weber, R.J., 2016. The characteristics of brown carbon aerosol during winter in Beijing. Atmos. Environ. 127, 355–364.

Claeys, M., Vermeylen, R., Yasmeen, F., Gomez-Gonzalez, Y., Chi, X., Maenhaut, W., Meszaros, Timea, Salma, I., 2012. Chemical characterisation of humic-like substances from urban, rural and tropical biomass burning environments using liquid chromatography with UV/VIS photodiode detection and electrospray ionisation mass spectrometry. Environ. Chem. 9, 273–284.

Cui, M., Chen, Y., Feng, Y., Li, C., Zheng, J., Tian, C., Yan, C., Zheng, M., 2017. Measurement of PM and its chemical composition in real-world emissions from non-road and on-road diesel vehicles. Atmos. Chem. Phys. 17, 6779–6795.

Cui, M., Chen, Y., Zheng, M., Li, J., Tang, J., Han, Y., Song, D., Yan, C., Zhang, F., Tian, C., Zhang, G., 2018. Emissions and characteristics of particulate matter from rainforest burning in the Southeast Asia. Atmos. Environ. 191, 194–204.

Dinar, E., Taraniuk, I., Graber, E.R., Anttila, T., Mentel, T.F., Rudich, Y., 2007. Hygroscopic growth of atmospheric and model humic-like substances. J. Geophys. Res. 112, D05211.

Dinar, E., Taraniuk, I., Graber, E.R., Katsman, S., Moise, T., Anttila, T., Mentel, T.F., Rudich, Y., 2006. Cloud Condensation Nuclei properties of model and atmospheric HULIS. Atmos. Chem. Phys. 6, 2465–2481.

Domeizel, M., Khalil, A., Prudent, P., 2004. UV spectroscopy: a tool for monitoring humification and for proposing an index of the maturity of compost. Bioresour. Technol. 94, 177–184.

Duarte, R., Santos, E.B.H., Pio, C.A., Duarte, A.C., 2007. Comparison of structural features of water-soluble organic matter from atmospheric aerosols with those of aquatic humic substances. Atmos. Environ. 41, 8100–8113.

Fan, X., Li, M., Cao, T., Cheng, C., Li, F., Xie, Y., Wei, S., Song, J., Peng, P.a., 2018. Optical properties and oxidative potential of water- and alkaline-soluble brown carbon in smoke particles emitted from laboratory simulated biomass burning. Atmos. Environ. 194, 48–57.

Fan, X., Song, J., Peng, P.a., 2012. Comparison of isolation and quantification methods to measure humic-like substances (HULIS) in atmospheric particles. Atmos. Environ. 60, 366–374.

Fan, X., Wei, S., Zhu, M., Song, J., Peng, P., 2016. Comprehensive characterization of humic-like substances in smoke $PM_{2.5}$ emitted from the combustion of biomass materials and fossil fuels. Atmos. Chem. Phys. 16, 13321–13340.

Ferek, R.J., Reid, J.G., Hobbs, P.V., Blake, D.R., Liousse, C., 1998. Emission factors of hydrocarbons, halocarbons, trace gases and particles from biomass burning in Brazil. J. Geophys. Res. 103, 32107–32118.

Graber, E.R., Rudich, Y., 2006. Atmospheric HULIS: how humic-like are they? A comprehensive and critical review. Atmos. Chem. Phys. 6, 729–753.

Guo, X.H., Da-Shi, Y.U., Wang, J., Tang, D.Y., Liu, X.M., 2008. Comparative study of the lignocellulose content in six plants. J. Hunan Univ. 76–78, 09.

Hecobian, A., Zhang, X., Zheng, M., Frank, N., Edgerton, E.S., Weber, R.J., 2010. Water-

Soluble Organic Aerosol material and the light-absorption characteristics of aqueous extracts measured over the Southeastern United States. Atmos. Chem. Phys. 10, 5965–5977.

Hoffer, A., Gelencsér, A., Guyon, P., Kiss, G., Schmid, O., Frank, G., Artaxo, P., Andreae, M., 2006. Optical properties of humic-like substances (HULIS) in biomass-burning aerosols. Atmos. Chem. Phys. 6, 3563–3570.

Hyer, E.J., Reid, J.S., 2009. Baseline uncertainties in biomass burning emission models resulting from spatial error in satellite active fire location data. Geophys. Res. Lett. 36, L05802.

Ito, A., Penner, J.E., 2004. Global estimates of biomass burning emissions based on satellite imagery for the year 2000. J. Geophys. Res. Atmos. 109, D14S05.

Jain, A.K., Tao, Z., Yang, X., Gillespie, C., 2006. Estimates of global biomass burning emissions for reactive greenhouse gases (CO, NMHCs, and NOx) and CO_2. J. Geophys. Res. Atmos. 111, D06304.

Jen, C.N., Hatch, L.E., Selimovic, V., Yokelson, R.J., Weber, R., Fernandez, A.E., Kreisberg, N.M., Barsanti, K.C., Goldstein, A.H., 2019. Speciated and total emission factors of particulate organics from burning western US wildland fuels and their dependence on combustion efficiency. Atmos. Chem. Phys. 19, 1013–1026.

Kiss, G., Varga, B., Galambos, I., Ganszky, I., 2002. Characterization of water-soluble organic matter isolated from atmospheric fine aerosol. J. Geophys. Res. Atmos. 107, 8339.

Kuang, B.Y., Lin, P., Huang, X.H.H., Yu, J.Z., 2015. Sources of humic-like substances in the Pearl River Delta, China: positive matrix factorization analysis of $PM_{2.5}$ major components and source markers. Atmos. Chem. Phys. 15, 1995–2008.

Kumar, V., Rajput, P., Goel, A., 2018. Atmospheric abundance of HULIS during wintertime in Indo-Gangetic Plain: impact of biomass burning emissions. J. Atmos. Chem. 75, 385–398.

Lee, H.-H., Bar-Or, R.Z., Wang, C., 2017. Biomass burning aerosols and the low-visibility events in Southeast Asia. Atmos. Chem. Phys. 17, 965–980.

Li, C., Yan, F., Kang, S., Chen, P., Hu, Z., Gao, S., Qu, B., Sillanpää, M., 2016. Light absorption characteristics of carbonaceous aerosols in two remote stations of the southern fringe of the Tibetan Plateau, China. Atmos. Environ. 143, 79–85.

Li, M., Fan, X., Zhu, M., Zou, C., Song, J., Wei, S., Jia, W., Peng, P., 2018. Abundances and light absorption properties of brown carbon emitted from residential coal combustion in China. Environ. Sci. Technol. 53, 595–603.

Lin, P., Engling, G., Yu, J.Z., 2010a. Humic-like substances in fresh emissions of rice straw burning and in ambient aerosols in the Pearl River Delta Region, China. Atmos. Chem. Phys. 10, 6487–6500.

Lin, P., Huang, X.-F., He, L.-Y., Zhen Yu, J., 2010b. Abundance and size distribution of HULIS in ambient aerosols at a rural site in South China. J. Aerosol. Sci. 41, 74–87.

Lin, P., Rincon, A.G., Kalberer, M., Yu, J.Z., 2012. Elemental composition of HULIS in the Pearl River Delta Region, China: results inferred from positive and negative electrospray high resolution mass spectrometric data. Environ. Sci. Technol. 46, 7454–7462.

Lin, P., Yu, J.Z., 2011. Generation of reactive oxygen species mediated by humic-like substances in atmospheric aerosols. Environ. Sci. Technol. 45, 10362–10368.

Liu, J., Bergin, M., Guo, H., King, L., Kotra, N., Edgerton, E., Weber, R.J., 2013. Size-resolved measurements of brown carbon in water and methanol extracts and estimates of their contribution to ambient fine-particle light absorption. Atmos. Chem. Phys. 13, 12389–12404.

Liu, J., Mo, Y., Ding, P., Li, J., Shen, C., Zhang, G., 2018. Dual carbon isotopes (^{14}C and ^{13}C) and optical properties of WSOC and HULIS-C during winter in Guangzhou, China. Sci. Total Environ. 633, 1571–1578.

Lu, Z., Streets, D.G., Winijkul, E., Yan, F., Chen, Y., Bond, T.C., Feng, Y., Dubey, M.K., Liu, S., Pinto, J.P., Carmichael, G.R., 2015. Light absorption properties and radiative effects of primary organic aerosol emissions. Environ. Sci. Technol. 49, 4868–4877.

Ma, H., Li, J., Wan, C., Liang, Y., Zhang, X., Dong, G., Hu, L., Yang, B., Zeng, X., Su, T., Lu, S., Chen, S., Khorram, M.S., Sheng, G., Wang, X., Mai, B., Yu, Z., Zhang, G., 2019. Inflammation response of water-soluble fractions in atmospheric fine particulates: a seasonal observation in 10 large Chinese cities. Environ. Sci. Technol. 53, 3782–3790.

Martinsson, J., Eriksson, A.C., Nielsen, I.E., Malmborg, V.B., Ahlberg, E., Andersen, C., Lindgren, R., Nystrom, R., Nordin, E.Z., Brune, W.H., Svenningsson, B., Swietlicki, E., Boman, C., Pagels, J.H., 2015. Impacts of combustion conditions and photochemical processing on the light absorption of biomass combustion aerosol. Environ. Sci. Technol. 49, 14663–14671.

Mcmeeking, G.R., Kreidenweis, S.M., Baker, S., Carrico, C.M., Chow, J.C., Collett, J.L., Hao, W.M., Holden, A.S., Kirchstetter, T.W., Malm, W.C., 2009. Emissions of trace gases and aerosols during the open combustion of biomass in the laboratory. J. Geophys. Res. 114, D19210.

Mo, Y., Li, J., Jiang, B., Su, T., Geng, X., Liu, J., Jiang, H., Shen, C., Ding, P., Zhong, G., Cheng, Z., Liao, X., Tian, C., Chen, Y., Zhang, G., 2018. Sources, compositions, and optical properties of humic-like substances in Beijing during the 2014 APEC summit: results from dual carbon isotope and Fourier-transform ion cyclotron resonance mass spectrometry analyses. Environ. Pollut. 239, 322–331.

Mo, Y.Z., Li, J., Liu, J.W., Zhong, G.C., Cheng, Z.N., Tian, C.G., Chen, Y.J., Zhang, G., 2017. The influence of solvent and pH on determination of the light absorption properties of water-soluble brown carbon. Atmos. Environ. 161, 90–98.

Nakata, M., Mukai, S., Yasumoto, M., 2018. Seasonal and regional characteristics of aerosol pollution in east and Southeast Asia. Front. Environ. Sci. 6, 29.

Nguyen, Q.T., Kristensen, T.B., Hansen, A.M.K., Skov, H., Bossi, R., Massling, A., Sørensen, L.L., Bilde, M., Glasius, M., Nøjgaard, J.K., 2014. Characterization of humic-like substances in Arctic aerosols. J. Geophys. Res. Atmos. 119,

5011–5027.

Park, S., Yu, G.-H., Lee, S., 2018. Optical absorption characteristics of brown carbon aerosols during the KORUS-AQ campaign at an urban site. Atmos. Res. 203, 16–27.

Park, S.S., Yu, J., 2016. Chemical and light absorption properties of humic-like substances from biomass burning emissions under controlled combustion experiments. Atmos. Environ. 136, 114–122.

Phillips, S.M., Smith, G.D., 2014. Light absorption by charge transfer complexes in Brown carbon aerosols. Environ. Sci. Technol. 1, 382–386.

Pokhrel, R.P., Wagner, N.L., Langridge, J.M., Lack, D.A., Jayarathne, T., Stone, E.A., Stockwell, C.E., Yokelson, R.J., Murphy, S.M., 2016. Parameterization of single-scattering albedo (SSA) and absorption Angstrom exponent (AAE) with EC/OC for aerosol emissions from biomass burning. Atmos. Chem. Phys. 16, 9549–9561.

Prasad, P., Roja Raman, M., Venkat Ratnam, M., Chen, W.-N., Vijaya Bhaskara Rao, S., Gogoi, M.M., Kompalli, S.K., Sarat Kumar, K., Suresh Babu, S., 2018. Characterization of atmospheric Black Carbon over a semi-urban site of Southeast India: local sources and long-range transport. Atmos. Res. 213, 411–421.

Roden, C.A., Bond, T.C., Conway, S., Benjamin, A., Pinel, O., 2006. Emission factors and real-time optical properties of particles emitted from traditional wood burning cookstoves. Environ. Sci. Technol. 40, 6750–6757.

Saleh, R., Hennigan, C.J., McMeeking, G.R., Chuang, W.K., Robinson, E.S., Coe, H., Donahue, N.M., Robinson, A.L., 2013. Absorptivity of brown carbon in fresh and photo-chemically aged biomass-burning emissions. Atmos. Chem. Phys. 13, 7683–7693.

Saleh, R., Robinson, E.S., Tkacik, D.S., Ahern, A.T., Liu, S., Aiken, A.C., Sullivan, R.C., Presto, A.A., Dubey, M.K., Yokelson, R.J., Donahue, N.M., Robinson, A.L., 2014. Brownness of organics in aerosols from biomass burning linked to their black carbon content. Nat. Geosci. 7, 647–650.

Salma, I., Mészáros, T., Maenhaut, W., Vass, E., Majer, Z., 2010. Chirality and the origin of atmospheric humic-like substances. Atmos. Chem. Phys. 10, 1315–1327.

Sengupta, D., Samburova, V., Bhattarai, C., Kirillova, E., Mazzoleni, L., Iaukea-Lum, M., Watts, A., Moosmüller, H., Khlystov, A., 2018. Light absorption by polar and non-polar aerosol compounds from laboratory biomass combustion. Atmos. Chem. Phys. 18, 10849–10867.

Shetty, N.J., Pandey, A., Baker, S., Hao, W.M., Chakrabarty, R.K., 2019. Measuring light absorption by freshly emitted organic aerosols: optical artifacts in traditional solvent-extraction-based methods. Atmos. Chem. Phys. 19, 8817–8830.

Shi, Y., Sasai, T., Yamaguchi, Y., 2014. Spatio-temporal evaluation of carbon emissions from biomass burning in Southeast Asia during the period 2001–2010. Ecol. Model. 272, 98–115.

Song, J., Li, M., Jiang, B., Wei, S., Fan, X., Peng, P., 2018. Molecular characterization of water-soluble humic like substances in smoke particles emitted from combustion of biomass materials and coal using ultrahigh-resolution electrospray ionization fourier transform ion cyclotron resonance mass spectrometry. Environ. Sci. Technol. 52, 2575–2585.

Stone, E.A., Hedman, C.J., Sheesley, R.J., Shafer, M.M., Schauer, J.J., 2009. Investigating the chemical nature of humic-like substances (HULIS) in North American atmospheric aerosols by liquid chromatography tandem mass spectrometry. Atmos. Environ. 43, 4205–4213.

Streets, D.G., Yarber, K.F., Woo, J.H., Carmichael, G.R., 2003. Biomass burning in Asia: annual and seasonal estimates and atmospheric emissions. Global Biogeochem. Cycles 17, 20.

Tan, J., Xiang, P., Zhou, X., Duan, J., Ma, Y., He, K., Cheng, Y., Yu, J., Querol, X., 2016. Chemical characterization of humic-like substances (HULIS) in $PM_{2.5}$ in Lanzhou, China. Sci. Total Environ. 573, 1481–1490.

Tang, J., Li, J., Su, T., Han, Y., Mo, Y., Jiang, H., Cui, M., Jiang, B., Chen, Y., Tang, J., Song, J., Peng, P., Zhang, G., 2020. Molecular compositions and optical properties of dissolved brown carbon in biomass burning, coal combustion, and vehicle emission aerosols illuminated by excitation–emission matrix spectroscopy and Fourier transform ion cyclotron resonance mass spectrometry analysis. Atmos. Chem. Phys. 20, 2513–2532.

Varga, B., Kiss, G., Ganszky, I., Gelencsér, A., Krivácsy, Z., 2001. Isolation of water-soluble organic matter from atmospheric aerosol. Talanta 55, 561–572.

Voliotis, A., Prokeš, R., Lammel, G., Samara, C., 2017. New insights on humic-like substances associated with wintertime urban aerosols from central and southern Europe: size-resolved chemical characterization and optical properties. Atmos. Environ. 166, 286–299.

Wang, Y., Hu, M., Lin, P., Guo, Q., Wu, Z., Li, M., Zeng, L., Song, Y., Zeng, L., Wu, Y., Guo, S., Huang, X., He, L., 2017. Molecular characterization of nitrogen-containing organic compounds in humic-like substances emitted from straw residue burning. Environ. Sci. Technol. 51, 5951–5961.

Ward, D.E., Radke, L.F., 1993. Emissions measurements from vegetation fires: a Comparative evaluation of methods and results. In: Crutzen, P.J., Goldammer, J.G. (Eds.), Fire in the Environment: the Ecological, Atmospheric and Climatic Importance of Vegetation Fires. John Wiley, New York, pp. 53–76.

Win, M.S., Tian, Z., Zhao, H., Xiao, K., Peng, J., Shang, Y., Wu, M., Xiu, G., Lu, S., Yonemochi, S., Wang, Q., 2018. Atmospheric HULIS and its ability to mediate the reactive oxygen species (ROS): a review. J. Environ. Sci. China 71, 13–31.

Xiang, P., Zhou, X., Duan, J., Tan, J., He, K., Yuan, C., Ma, Y., Zhang, Y., 2017. Chemical characteristics of water-soluble organic compounds (WSOC) in $PM_{2.5}$ in Beijing, China: 2011–2012. Atmos. Res. 183, 104–112.

Xie, M., Chen, X., Holder, A.L., Hays, M.D., Lewandowski, M., Offenberg, J.H., Kleindienst, T.E., Jaoui, M., Hannigan, M.P., 2019. Light absorption of organic

carbon and its sources at a southeastern U.S. location in summer. Environ. Pollut. 244, 38–46.

Xie, M., Hays, M.D., Holder, A.L., 2017. Light-absorbing organic carbon from prescribed and laboratory biomass burning and gasoline vehicle emissions. Sci. Rep. 7, 7318.

Yokelson, R.J., Susott, R., Ward, D.E., Reardon, J., Griffith, D.W.T., 1997. Emissions from smoldering combustion of biomass measured by open-path Fourier transform infrared spectroscopy. J. Geophys. Res. Atmos. 102, 18865–18877.

Zhang, X., Lin, Y.H., Surratt, J.D., Weber, R.J., 2013a. Sources, composition and absorption Angstrom exponent of light-absorbing organic components in aerosol extracts from the Los Angeles Basin. Environ. Sci. Technol. 47, 3685–3693.

Zhang, Y., Shao, M., Lin, Y., Luan, S., Mao, N., Chen, W., Wang, M., 2013b. Emission inventory of carbonaceous pollutants from biomass burning in the Pearl River Delta Region, China. Atmos. Environ. 76, 189–199.

Zheng, G., He, K., Duan, F., Cheng, Y., Ma, Y., 2013. Measurement of humic-like substances in aerosols: a review. Environ. Pollut. 181, 301–314.

Zhou, X., Zhang, L., Tan, J., Zhang, K., Mao, J., Duan, J., Hu, J., 2018. Characterization of humic-like substances in $PM_{2.5}$ during biomass burning episodes on Weizhou Island, China. Atmos. Environ. 191, 258–266.